Acta Mech 229, 2631–2646 (2018)
https://doi.org/10.1007/s00707-018-2114-6

ORIGINAL PAPER

Shivakumar I. Ranganathan · Muhammad Ridwan Murshed · Luis Costa

Heterogeneous Anisotropy Index and scaling in two-phase random polycrystals

Received: 16 July 2017 / Revised: 16 December 2017 / Published online: 1 March 2018

Abstract Under consideration is the finite-size scaling of the elastic properties in two-phase random polycrystals with individual grains belonging to any arbitrary crystal class. These polycrystals are generated by Voronoi Tessellations with varying grain sizes and volume fractions. Any given realization of such a microstructure sampled randomly is highly anisotropic and heterogeneous. Using extremum principles in elasticity, we introduce the notion of a 'Heterogeneous Anisotropy Index $\left(A_H^U\right)$' and examine its role in the scaling of elastic properties at finite mesoscales (δ). The relationship between A_H^U and the Universal Anisotropy Index A^U by Ranganathan and Ostoja-Starzewski (Phys Rev Lett 101(5):055504, 2008) is established for special cases. The index A_H^U turns out to be a function of 43 variables—21 independent components for each phase and the volume fraction of either phase. The scale-dependent bounds are then obtained by setting up and solving 9250 Dirichlet and Neumann type boundary value problems consistent with the Hill–Mandel homogenization condition. Subsequently, the concept of an elastic scaling function is introduced that takes a power-law form in terms of A_H^U and (δ). Finally, a material scaling diagram is constructed by employing the elastic scaling function which captures the convergence to the effective properties for any two-phase elastic microstructure.

1 Introduction

Polycrystalline materials have unique properties and are commonly used in several engineering applications (such as elasticity [2], heat conduction [3], fracture [4,5], magnetism [6]). In particular, two-phase polycrystals have been used in minerals engineering [7], thermal conductivity [8], plasticity [9]. Such materials have grains belonging to any crystal class (from cubic to triclinic) with arbitrary orientations. These microstructures are highly anisotropic and heterogeneous at finite scales, thereby posing a challenge to the predictive modeling of their collective behavior. The objective of this research is to introduce the notion of a 'Heterogeneous Anisotropy Index' and examine its role in the finite-size scaling of two-phase random polycrystals.

In the past, several authors have investigated the effective response of two-phase materials and some of these are noteworthy. In particular, Hashin and Shtrikman [10] used variational principles to illustrate upper and lower bounds on elastic moduli of two-phase materials. In their study, the authors analyzed a two-phase

S. I. Ranganathan (✉)
Department of Mechanical Engineering, Virginia Polytechnic Institute and State University, Northern Virginia Center, Room 434, 7054 Haycock Road, Falls Church, VA 22043, USA
E-mail: srangan3@vt.edu

M. R. Murshed
Department of Mechanical Engineering, Rowan University, 201 Mullica Hill Road, Glassboro, NJ 08028, USA

L. Costa
Institute for Multiscale Reactive Modeling, Energetics and Warheads Research and Development, RDAR-MEE-W, Building 3022, Room 44, Picatinny, NJ 07806-5000, USA

alloy (Tungsten Carbide) and proved that their theoretical results were in good agreement with experimental results. Along similar lines, Walpole [11] examined upper and lower bounds as well as self-consistent estimates on the elastic moduli of materials. The author developed theoretical expressions for shear and bulk moduli of composites with transversely isotropic inclusions (needle or disk shape) at random orientations and arbitrary volume fractions. Similarly, Watt et al. [12] analyzed bounds on shear and bulk moduli of several two-phase composites with different volume fractions ($v_f = 0, 0.2, 0.4, 0.8, 1$). It was demonstrated that the effective moduli of these materials were within Hashin–Shtrikman bounds for all volume fractions.

An alternate approach to determine the effective properties is to employ the Mori–Tanaka method (see Mori and Tanaka [13]) that relates the average stress in an inclusion to the average stress in the matrix in multiphase composites. Benveniste [14] analyzed two-phase materials with anisotropic elastic constituents by reformulating the Mori–Tanaka method in order to determine the aggregate response. In the study, the author illustrated that shear and bulk moduli for two-phase composites were within Hashin–Shtrikman bounds. Along similar lines, Weng [15] analyzed the relationship between Hashin–Shtrikman–Walpole (H–S–W) bounds and the Mori–Tanaka (M–T) method for composites. The author investigated multiphase materials with unidirectionally aligned constituents and observed the following: (i) For spherical inclusions, M–T moduli will always fall within H–S–W bounds when the matrix is neither the softest nor the hardest phase; (ii) For circular fibers, the M–T method will lie within the H–S–W bounds like the spherical case; (iii) For thin disks, M–T moduli will be an exact solution like the H–S–W bounds (upper and lower bounds coincide as these are independent of the material property).

More recently, Ni and Chiang [16] predicted the effective elastic constants of two-phase isotropic materials. In their work, the authors used phase-field microelasticity (PFM) that is based on Eshelby's effective eigenstrain approach (see Eshelby [17]) in order to obtain the elastic properties at specific volume fractions ($v_f = 0.1$, $0.2, 0.3, 0.4, 0.5$). It was shown that PFM method can be employed only for lower volume fractions ($v_f < 0.2$) to estimate shear and bulk moduli.

An alternative method for studying the effective response of materials is to employ the Hill–Mandel homogenization condition (see Hill [18] and Mandel [19]). In this approach, the constitutive response of elastic polycrystals at finite scales is obtained by solving Dirichlet and Neumann type boundary value problems that bound the response from above and below, respectively. The microstructure is assumed to be spatially homogeneous, ergodic and with increasing length scales, the microstructure moves from a so-called Statistical Volume Element (SVE) to a Representative Volume Element (RVE). The versatility of this methodology is evident from the fact that it has attracted a great deal of interest over the past several decades within the context of elasticity [20–22], thermal conductivity [23–25], thermoelasticity [26–28], flow in porous media [29,30], fracture and damage phenomena in random microstructures [31] and nonlinear elastic and inelastic materials [32,33]. This framework has been employed by several other authors in order to determine the effective response of two-phase polycrystals. In particular, Kanit et al. [34] analyzed three-dimensional Voronoi mosaic-shaped linearly elastic materials in order to determine the effective properties of two-phase microstructures. In their work, the authors used several boundary conditions (Dirichlet and Neumann) and obtained shear and bulk moduli of two-phase materials at a specific volume fraction ($v_f = 0.7$). The authors also observed that their elastic moduli were within Voigt–Reuss [35,36] (upper bound and lower bound) as well as Hashin–Shtrikman bounds. Along similar lines, Kanit et al. [37] investigated real two-phase microstructures using a digital representation of their morphology and obtained the effective response. In their study, the authors analyzed 3D confocal images of polycrystalline ice and polymeric cream which were phase 1 and phase 2, respectively. Subsequently, the authors performed numerical simulations using Dirichlet and Neumann boundary conditions on two-phase microstructures and showed that shear and bulk moduli were within Voigt–Reuss as well as Hashin–Shtrikman bounds.

Several other authors have also employed the Hill–Mandel homogenization condition to demonstrate the concept of a scaling function. This function unifies the treatment of a wide variety of materials by describing the effective response of random polycrystals through the convergence of Dirichlet and Neumann bounds. Recently, the scaling function has been studied in 3D elasticity (for individual grains belonging to any crystal class from cubic to triclinic) [38] and previously in 3D heat conduction [39], 2D elasticity [40], 2D heat conduction [41], 2D electrical conductivity [42] and 2D viscoelasticity [43].

In the subsequent sections, we generate two-phase random polycrystals by Voronoi Tessellations and the microstructures considered in this study have real-world applications. For instance, Ni–Cd is used in batteries [44], Sn–Ag is used for soldering joints [45], Ni–Cr is employed for strain gauge applications [46], and Ni–Co is used as a corrosion resistant coating [47]. We then vary the grain sizes (25, 400, 1000, 5000 grains) at different volume fractions ($v_f = 0, 0.25, 0.5, 0.75, 1$) in order to obtain rigorous bounds at finite mesoscales

as solutions to stochastic boundary value problems (Dirichlet and Neumann) consistent with the Hill–Mandel homogenization condition. By analyzing 9250 boundary value problems, it will be demonstrated that these bounds converge to the effective elastic properties with increasing number of grains. We also illustrate the notion of an elastic scaling function which depends on the 'Heterogeneous Anisotropy Index' and the number of grains in the domain. Finally, a material scaling diagram is constructed that enables one to estimate the number of grains required for homogenization of two-phase random microstructures.

2 Mathematical formulation

2.1 Hill–Mandel homogenization condition

In this section, we illustrate the Hill–Mandel homogenization condition which employs the energetic and mechanistic approaches for setting up constitutive equations (see Hill [18] and Mandel [19]). First, we discuss the stress and strain fields ($\boldsymbol{\sigma}$ and $\boldsymbol{\varepsilon}$) and decompose these terms into mean and fluctuating parts as follows (see Ostoja-Starzewski [31])

$$\begin{aligned} \boldsymbol{\sigma}(\mathbf{x},\omega) &= \bar{\boldsymbol{\sigma}}(\omega) + \boldsymbol{\sigma}'(\mathbf{x},\omega), \\ \boldsymbol{\varepsilon}(\mathbf{x},\omega) &= \bar{\boldsymbol{\varepsilon}}(\omega) + \boldsymbol{\varepsilon}'(\mathbf{x},\omega), \end{aligned} \tag{2.1}$$

where $\mathbf{x}$ is the point-to-point dependence of fluctuating fields, $\omega(\in \Omega)$ refers to a particular realization in a microstructure from the sample space, Ω, and an over-bar is used to represent the volume average. Equation (2.1) is separated into the mean and zero-mean fluctuations as follows (see Ostoja-Starzewski [31])

$$\begin{aligned} \bar{\boldsymbol{\sigma}}_\delta(\omega) &= \frac{1}{V}\int \boldsymbol{\sigma}(\mathbf{x},\omega)\mathrm{d}V, \quad \int \boldsymbol{\sigma}'(\mathbf{x},\omega)\mathrm{d}V = 0, \\ \bar{\boldsymbol{\varepsilon}}_\delta(\omega) &= \frac{1}{V}\int \boldsymbol{\varepsilon}(\mathbf{x},\omega)\mathrm{d}V, \quad \int \boldsymbol{\varepsilon}'(\mathbf{x},\omega)\mathrm{d}V = 0. \end{aligned} \tag{2.2}$$

Here, V is the volume of the microstructure and δ is the mesoscale which can be defined as (see Ranganathan and Ostoja-Starzewski [20])

$$\delta = \frac{l}{d} = (N_G)^{\frac{1}{3}}, \tag{2.3}$$

where N_G is the number of grains in the microstructure, d is the characteristic length scale (for example the grain size), and l is the length scale of observation (domain size). Using Eqs. (2.1) and (2.2), the volume-averaged contracted scalar product of $\boldsymbol{\sigma}$ and $\boldsymbol{\varepsilon}$ is defined as

$$\overline{\sigma_{ij}\varepsilon_{ij}} = \frac{1}{V}\int_V \sigma_{ij}\varepsilon_{ij}\mathrm{d}V = \bar{\sigma}_{ij}\bar{\varepsilon}_{ij} + \frac{1}{V}\int_V \sigma'_{ij}\varepsilon'_{ij}\mathrm{d}V. \tag{2.4}$$

We now illustrate the Hill–Mandel condition which follows from Eq. (2.4) as

$$\overline{\sigma_{ij}\varepsilon_{ij}} = \bar{\sigma}_{ij}\bar{\varepsilon}_{ij}. \tag{2.5}$$

The relation Eq. (2.5) holds provided the following condition is satisfied:

$$\frac{1}{V}\int_V \boldsymbol{\sigma}' : \boldsymbol{\varepsilon}'\mathrm{d}V = 0. \tag{2.6}$$

Now, by employing Eq. (2.1) and applying the Green–Gauss theorem to Eq. (2.6), we obtain the following (see Ranganathan and Ostoja-Starzewski [20]):

$$\frac{1}{V}\int_V \sigma'_{ij}\varepsilon'_{ij}\mathrm{d}V = 0 \Leftrightarrow \int_{\partial B_\delta} (t_i - \overline{\sigma_{ij}}.n_j)(u_i - \overline{\varepsilon_{ij}}.x_j)dS = 0, \tag{2.7}$$

where B_δ is the random mesoscale material ($B_\delta = B_\delta(\omega); \omega \in \Omega$) with a single deterministic realization denoted by $B_\delta(\omega)$ (see Ostoja-Starzewski et al. [2]). In addition, ∂B_δ is the boundary of B_δ (see Ostoja-Starzewski [31]).

At this stage, we show the three types of boundary conditions that are obtained using Eq. (2.7) as follows (see Ostoja-Starzewski et al. [2], Ranganathan and Ostoja-Starzewski [21] and Hill [48]):

(i) Uniform Displacement (Dirichlet)

$$u_i = \varepsilon^0_{ij} x_j \tag{2.8a}$$

(ii) Uniform Traction (Neumann)

$$t_i = \sigma^0_{ij} n_j \tag{2.8b}$$

(iii) Mixed-orthogonal

$$\left(t_i - \sigma^0_{ij} n_j\right)\left(u_i - \varepsilon^0_{ij} x_j\right) = 0 \tag{2.8c}$$

One can now set up stochastic boundary value problems with the above boundary conditions and, upon ensemble averaging, the mesoscale effective response can be obtained. It has to be noted that the random field, $\boldsymbol{\Theta}(\mathbf{x})$, of material parameters involved must be spatially homogeneous and ergodic. The ensemble mean is constant, and its finite-valued covariance depends only on the shift $\mathbf{h}$ from $\mathbf{x}$ to $\mathbf{x}+\mathbf{h}$ (see Ostoja-Starzewski [28]),

$$\begin{aligned} \langle \boldsymbol{\Theta}(\mathbf{x}) \rangle &= \mu, \\ \langle [\boldsymbol{\Theta}(\mathbf{x}) - \langle \boldsymbol{\Theta}(\mathbf{x}) \rangle][\boldsymbol{\Theta}(\mathbf{x}+\mathbf{h}) - \langle \boldsymbol{\Theta}(\mathbf{x}+\mathbf{h}) \rangle] \rangle &= K_{\boldsymbol{\Theta}}(\mathbf{h}) < \infty, \end{aligned} \tag{2.9}$$

where $\boldsymbol{\Theta}(\mathbf{x})$ is a wide-sense stationary (WSS) random field, $K_{\boldsymbol{\Theta}}(\mathbf{h})$ is the covariance function, and the ensemble averages are represented by $\langle \cdot \rangle$. We also observe that the random field $\boldsymbol{\Theta}(\mathbf{x})$ outlined above is mean-ergodic if the spatial average (denoted by the over-bar) is equal to the ensemble average (see Ostoja-Starzewski [28])

$$\frac{1}{V}\int_V \boldsymbol{\Theta}(\omega, \mathbf{x}) \mathrm{d}V = \overline{\boldsymbol{\Theta}(\omega)} = \langle \boldsymbol{\Theta}(\mathbf{x}) \rangle = \int_\Omega \boldsymbol{\Theta}(\omega, \mathbf{x}) dP, \tag{2.10}$$

where P is a probability measure related to the random field $\boldsymbol{\Theta}(\mathbf{x})$. The homogenization methodology can be seen in Fig. 1 where each grain has a random orientation. The polycrystals are generated by Voronoi Tessellations using the software Neper (see Quey et al. [49]) and the grain sizes ($N_G = 25, 400, 1000, 5000$) that are taken into consideration are based on the work by El Houdaigui et al. [50]. Subsequently, Dirichlet and Neumann boundary value problems are solved using Eqs. (2.8a) and (2.8b) and the scale-dependent bounds are obtained on the elastic response of two-phase random polycrystals. In the next section, we postulate a specific form of the scaling function for two-phase materials.

2.2 Elastic scaling function

Consider an arbitrary realization $B_\delta(\omega)$ of a random medium B_δ on a specific mesoscale δ. By using Eq. (2.8a), a mesoscale random stiffness tensor $\mathbf{C}^d_\delta$ can be defined as (see Ostoja-Starzewski [31])

$$\bar{\boldsymbol{\sigma}}_\delta(\omega) = \mathbf{C}^d_\delta(\omega) : \boldsymbol{\varepsilon}^0, \tag{2.11}$$

where the superscript d denotes the displacement boundary condition (see Ostoja-Starzewski et al. [2]). Along similar lines, Eq. (2.8b) yields a mesoscale random compliance tensor $\mathbf{S}^t_\delta$ as follows (see Ostoja-Starzewski [31]):

$$\bar{\boldsymbol{\varepsilon}}_\delta(\omega) = \mathbf{S}^t_\delta(\omega) : \boldsymbol{\sigma}^0 \tag{2.12}$$

and the superscript t denotes the uniform traction boundary condition (see Ostoja-Starzewski et al. [2]). In general, $\mathbf{C}$ and $\mathbf{S}$ are anisotropic at finite mesoscales. Isotropic response can only be recovered by distributing the single crystal orientation randomly and upon ensemble averaging. The isotropic forms of the stiffness and compliance tensors in terms of the bulk modulus, K, as well as the shear modulus, G, can be represented as follows (see Ranganathan and Ostoja-Starzewski [21]):

$$\left\langle \mathbf{C}^d_\delta \right\rangle = 2\left\langle G^d_\delta \right\rangle \mathbf{K} + 3\left\langle K^d_\delta \right\rangle \mathbf{J}, \tag{2.13a}$$

$$\left\langle \mathbf{S}^t_\delta \right\rangle = \frac{1}{2\left\langle G^t_\delta \right\rangle}\mathbf{K} + \frac{1}{3\left\langle K^t_\delta \right\rangle}\mathbf{J}, \tag{2.13b}$$

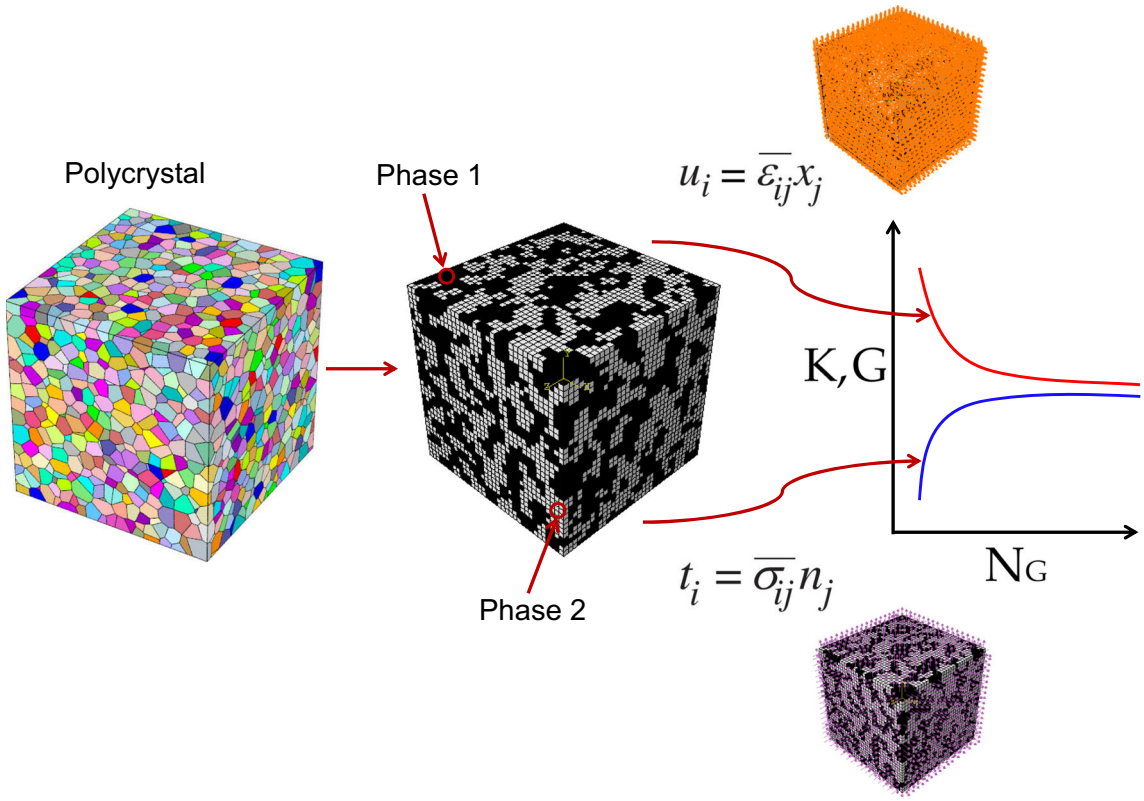

Fig. 1 The homogenization methodology

where **K** and **J** are the deviatoric and spherical components (introduced by Walpole [51,52]) of the fourth-order identity tensor, **I**. We now define **I** as follows (see Hill [53], Walpole [52], Ranganathan et al. [54])

$$\mathbf{I} = I_{ijkl} e_i \otimes e_j \otimes e_k \otimes e_l = \frac{\delta_{il}\delta_{jk} + \delta_{ik}\delta_{jl}}{2} e_i \otimes e_j \otimes e_k \otimes e_l, \tag{2.14}$$

where δ_{ij} is the Kronecker Δ with $\delta_{ij} = 1$ when $i = j$ and $\delta_{ij} = 0$ when $i \neq j$. Let us now consider the spherical component, **J**, of the fourth-order tensor **I** as follows (see Hill [53], Walpole [52], Ranganathan et al. [54]):

$$\mathbf{J} = J_{ijkl} e_i \otimes e_j \otimes e_k \otimes e_l = \frac{\delta_{ij}\delta_{kl}}{3} e_i \otimes e_j \otimes e_k \otimes e_l. \tag{2.15}$$

Also, $\mathbf{K} = \mathbf{I} - \mathbf{J}$. By quadruple contraction of Eqs. (2.13a) and (2.13b), we obtain the following scalar equation (see Itskov [55] and Ranganathan and Ostoja-Starzewski [21]):

$$\begin{aligned} \left\langle \mathbf{C}_\delta^d \right\rangle :: \left\langle \mathbf{S}_\delta^t \right\rangle &= \left\langle C_{ijkl} e_i \otimes e_j \otimes e_k \otimes e_l \right\rangle :: \left\langle S_{mnrs} e_m \otimes e_n \otimes e_r \otimes e_s \right\rangle \\ &= \left\langle C_{ijkl} S_{jilk} \right\rangle = 5 \frac{\left\langle G_\delta^d \right\rangle}{\left\langle G_\delta^t \right\rangle} + \frac{\left\langle K_\delta^d \right\rangle}{\left\langle K_\delta^t \right\rangle}. \end{aligned} \tag{2.16}$$

By taking the limit ($\delta \to \infty$), the stiffness tensor is the exact inverse of the compliance tensor as follows (see Ranganathan and Ostoja-Starzewski [21]):

$$\lim_{\delta \to \infty} \left\langle \mathbf{C}_\delta^d \right\rangle :: \left\langle \mathbf{S}_\delta^t \right\rangle = 6. \tag{2.17}$$

Rearranging Eqs. (2.16) and (2.17), we postulate the following relationship:

$$\left\langle \mathbf{C}_\delta^d \right\rangle :: \left\langle \mathbf{S}_\delta^t \right\rangle = \lim_{\delta \to \infty} \left\langle \mathbf{C}_\delta^d \right\rangle :: \left\langle \mathbf{S}_\delta^t \right\rangle + f(C_{(1)}^{ij}, C_{(2)}^{ij}, v_f, \delta), \tag{2.18}$$

where $f\left(C^{ij}_{(1)}, C^{ij}_{(2)}, v_f, \delta\right)$ is the non-dimensional function called the elastic scaling function and v_f is the volume fraction of phase 1. Equation (2.18) is applicable for two-phase materials unlike the scaling function first proposed by Ranganathan and Ostoja-Starzewski [20] for single phase cubic crystals. The variable C^{ij} represents all the single crystal elastic constants depending on the crystal class and applies to both $C^{ij}_{(1)}$ (phase 1) and $C^{ij}_{(2)}$ (phase 2) as given below:

(i) Cubic

$$C^{ij} \equiv (C_{11}, C_{12}, C_{44}), \tag{2.19a}$$

(ii) Hexagonal

$$C^{ij} \equiv (C_{11}, C_{12}, C_{13}, C_{33}, C_{44}), \tag{2.19b}$$

(iii) Tetragonal

$$C^{ij} \equiv (C_{11}, C_{12}, C_{13}, C_{33}, C_{44}, C_{66}), \tag{2.19c}$$

(iv) Trigonal

$$C^{ij} \equiv (C_{11}, C_{12}, C_{13}, C_{14}, C_{33}, C_{44}), \tag{2.19d}$$

(iv) Orthorhombic

$$C^{ij} \equiv (C_{11}, C_{12}, C_{13}, C_{22}, C_{23}, C_{33}, C_{44}, C_{55}, C_{66}), \tag{2.19e}$$

(v) Monoclinic

$$C^{ij} \equiv (C_{11}, C_{12}, C_{13}, C_{15}, C_{22}, C_{23}, C_{25}, C_{33}, C_{35}, C_{44}, C_{46}, C_{55}, C_{66}), \tag{2.19f}$$

(vi) Triclinic

$$\begin{aligned} C^{ij} \equiv (&C_{11}, C_{12}, C_{13}, C_{14}, C_{15}, C_{16}, C_{22}, C_{23}, C_{24}, C_{25}, C_{26}, \\ &C_{33}, C_{34}, C_{35}, C_{36}, C_{44}, C_{45}, C_{46}, C_{55}, C_{56}, C_{66}). \end{aligned} \tag{2.19g}$$

Substituting Eqs. (2.17) and (2.18) into Eq. (2.16) gives the functional form of the elastic scaling function as

$$f(C^{ij}_{(1)}, C^{ij}_{(2)}, v_f, \delta) = 5\frac{\langle G^d_\delta \rangle}{\langle G^t_\delta \rangle} + \frac{\langle K^d_\delta \rangle}{\langle K^t_\delta \rangle} - 6. \tag{2.20}$$

The boundary value problems listed under Eqs. (2.8a) and (2.8b) can be solved numerically in order to obtain the right hand side of Eq. (2.20). In the next section, we discuss the upper and lower bounds on the elastic property (bulk and shear moduli) of materials.

2.3 Bounds on the bulk and shear moduli

The hierarchy of scale-dependent bounds on the elastic response of random microstructures is shown by employing the spatial ergodicity, WSS properties and the variational principles of continuum elasticity as follows (see Ostoja-Starzewski [31], Kanit et al. [34], Sab [56], Huet [57]):

$$\langle \mathbf{S}^t_1 \rangle^{-1} \leq \cdots \leq \langle \mathbf{S}^t_{\delta'} \rangle^{-1} \leq \langle \mathbf{S}^t_{\delta} \rangle^{-1} \leq \cdots \leq \mathbf{C}^{eff}_\infty \ldots \leq \left\langle \mathbf{C}^d_\delta \right\rangle \leq \left\langle \mathbf{C}^d_{\delta'} \right\rangle \cdots \leq \left\langle \mathbf{C}^d_1 \right\rangle \ \forall \delta' \leq \delta. \tag{2.21}$$

By using Eq. (2.21), the hierarchy of bounds on the bulk and shear moduli for isotropic stiffness tensors can be seen as follows (see Ranganathan and Ostoja-Starzewski [21] and Ostoja-Starzewski et al. [2]):

$$K^R \leq \cdots \leq \langle K^t_{\delta'} \rangle \leq \langle K^t_{\delta} \rangle \leq \cdots \leq K^{eff}_\infty \ldots \leq \left\langle K^d_\delta \right\rangle \leq \left\langle K^d_{\delta'} \right\rangle \cdots \leq K^V \quad \forall \delta' \leq \delta, \tag{2.22a}$$

$$G^R \leq \cdots \leq \langle G^t_{\delta'} \rangle \leq \langle G^t_{\delta} \rangle \leq \cdots \leq G^{eff}_\infty \ldots \leq \left\langle G^d_\delta \right\rangle \leq \left\langle G^d_{\delta'} \right\rangle \cdots \leq G^V \quad \forall \delta' \leq \delta, \tag{2.22b}$$

where K^V and K^R are the Voigt and Reuss estimates for the bulk modulus, respectively (see Hill [58]). Similarly, G^V and G^R are the Voigt and Reuss bounds for the shear modulus. In the subsequent section, we illustrate the properties and bounds on the scaling function.

2.4 Properties and bounds on the elastic scaling function

The elastic scaling function $f\left(C^{ij}_{(1)}, C^{ij}_{(2)}, v_f, \delta\right)$ which is postulated in Eq. (2.18) has the following properties:

$$f\left(C^{ij}_{(1)}, C^{ij}_{(2)}, v_f, \delta \to \infty\right) = 0, \tag{2.23}$$

where the scaling function is equal to zero at infinite mesoscales. Also, if $C^{ij}_{(1)}$ and $C^{ij}_{(2)}$ are changed to $\alpha\, C^{ij}_{(1)}$ and $\alpha\, C^{ij}_{(2)}$ (α is a real number), the scaling function f remains the same:

$$f\left(\alpha\, C^{ij}_{(1)}, \alpha\, C^{ij}_{(2)}, v_f, \delta\right) = f\left(C^{ij}_{(1)}, C^{ij}_{(2)}, v_f, \delta\right). \tag{2.24}$$

Next, the bounds of the elastic scaling function can be seen as follows:

$$\begin{aligned} f\left(C^{ij}_{(1)}, C^{ij}_{(2)}, v_f, \delta \to \infty\right) \le f\left(C^{ij}_{(1)}, C^{ij}_{(2)}, v_f, \delta'\right) \le f\left(C^{ij}_{(1)}, C^{ij}_{(2)}, v_f, \delta\right) \\ \cdots \le f\left(C^{ij}_{(1)}, C^{ij}_{(2)}, v_f, \delta = 1\right) \quad \forall 1 \le \delta \le \delta' \le \infty. \end{aligned} \tag{2.25}$$

One can now postulate several forms of the scaling function by identifying the appropriate parameters of f. In the subsequent section, the notion of 'Heterogeneous Anisotropy Index' is introduced that is a natural consequence of Eq. (2.25).

2.5 Heterogeneous Anisotropy Index

The 'Heterogeneous Anisotropy Index,' A^U_H, which is obtained from Eq. (2.25), can be defined as follows:

$$A^U_H = f\left(C^{ij}_{(1)}, C^{ij}_{(2)}, v_f, \delta = 1\right) \quad 0 \le v_f \le 1, \tag{2.26a}$$

where

$$\begin{aligned} A^U_H &= a + b v_f + c v_f^2, \\ a &= 5\frac{G^V_{(2)}}{G^R_{(2)}} + \frac{K^V_{(2)}}{K^R_{(2)}} - 6, \\ b &= 5\left[\frac{G^V_{(1)}}{G^R_{(2)}} + \frac{G^V_{(2)}}{G^R_{(1)}} - \frac{2G^V_{(2)}}{G^R_{(2)}}\right] + \frac{K^V_{(1)}}{K^R_{(2)}} + \frac{K^V_{(2)}}{K^R_{(1)}} - \frac{2K^V_{(2)}}{K^R_{(2)}}, \\ c &= 5\left[\frac{G^V_{(1)}}{G^R_{(1)}} - \frac{G^V_{(1)}}{G^R_{(2)}} - \frac{G^V_{(2)}}{G^R_{(1)}} + \frac{G^V_{(2)}}{G^R_{(2)}}\right] + \frac{K^V_{(1)}}{K^R_{(1)}} - \frac{K^V_{(1)}}{K^R_{(2)}} - \frac{K^V_{(2)}}{K^R_{(1)}} + \frac{K^V_{(2)}}{K^R_{(2)}}, \end{aligned} \tag{2.26b}$$

and the subscripts (1) and (2) represent phase 1 and phase 2, respectively. The 'Heterogeneous Anisotropy Index' captures the anisotropy of each phase in a two-phase material at arbitrary volume fractions ($0 \le v_f \le 1$). It can also be seen that, when the volume fraction of phase 1 is zero, we observe the following:

$$f\left(C^{ij}_{(1)}, C^{ij}_{(2)}, v_f = 0, \delta = 1\right) = a = A^U_{(2)} \ge 0, \tag{2.27}$$

where $A^U_{(2)}$ is anisotropy of phase 2 only (single phase) and can be represented by the Universal Anisotropy Index, A^U, of this phase (see Ranganathan and Ostoja-Starzewski [1]). Similarly, when the volume fraction of phase 1 is one, we obtain the following:

$$f\left(C^{ij}_{(1)}, C^{ij}_{(2)}, v_f = 1, \delta = 1\right) = a + b + c = A^U_{(1)} \ge 0 \tag{2.28}$$

and $A^U_{(1)}$ is anisotropy of phase 1 which is again a single phase material. Let us now discuss Fig. 2 which illustrates the 'Heterogeneous Anisotropy Index' of 4 two-phase materials (Ni–Cd, Sn–Ag, Ni–Cr, Ni–Co) at

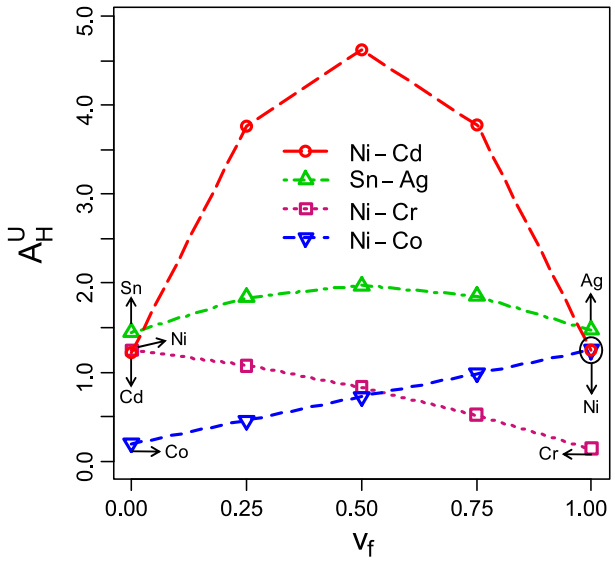

Fig. 2 Heterogeneous Anisotropy Index (A_H^U) versus volume fraction (v_f) for two-phase materials (Ni–Cd, Sn–Ag, Ni–Cr, Ni–Co)

different volume fractions ($v_f = 0, 0.25, 0.5, 0.75, 1$). We observe for Ni–Cd that A_H^U is similar at $v_f = 0.25$ as well as $v_f = 0.75$, and therefore, scaling behavior is expected to be same at these volume fractions (see Fig. 2). A similar phenomenon can be seen for Sn–Ag as A_H^U is identical at $v_f = 0.25$ and $v_f = 0.75$. For Ni–Cr, A_H^U decreases from $A_H^U = 1.25$ to $A_H^U = 0.14$ with an increase in volume fraction from $v_f = 0$ to $v_f = 1$ (see Fig. 2). An opposite trend can be observed in Fig. 2 for Ni–Co as A_H^U increases from $A_H^U = 0.2$ to $A_H^U = 1.25$ with an increase in volume fraction. In the next section, the constitutive response of elastic polycrystals at finite scales is obtained by solving Dirichlet and Neumann type boundary value problems:

3 Results and discussion

Consider the rigorous bounds on elastic constants of two-phase random polycrystals at finite mesoscales. These polycrystals are white-noise random fields as these have no spatial correlations. Also, these microstructures are generated numerically according to spatially ergodic and WSS properties. In the subsequent sections, we study 4 two-phase materials at different volume fractions ($v_f = 0, 0.25, 0.5, 0.75, 1$) and perform 9250 numerical simulations in order to illustrate the scale-dependent bounds on the effective elastic response (shear and bulk moduli). In doing so, we impose the following loading conditions to solve stochastic boundary value problems

(1) Dirichlet problem:
   (i) For extracting shear modulus: $\varepsilon_{11}^0 = \varepsilon_{22}^0 = 0.05,\ \varepsilon_{33}^0 = -0.1,\ \varepsilon_{12}^0 = \varepsilon_{13}^0 = \varepsilon_{23}^0 = 0$;
   (ii) For extracting bulk modulus: $\varepsilon_{11}^0 = \varepsilon_{22}^0 = \varepsilon_{33}^0 = 0.05,\ \varepsilon_{12}^0 = \varepsilon_{13}^0 = \varepsilon_{23}^0 = 0$;
(2) Neumann problem:
   (iii) For extracting shear modulus: $\sigma_{11}^0 = \sigma_{22}^0 = 16$ GPa, $\sigma_{33}^0 = -32$ GPa, $\sigma_{12}^0 = \sigma_{13}^0 = \sigma_{23}^0 = 0$;
   (iv) For extracting bulk modulus: $\sigma_{11}^0 = \sigma_{22}^0 = \sigma_{33}^0 = 16$ GPa, $\sigma_{12}^0 = \sigma_{13}^0 = \sigma_{23}^0 = 0$.

Next, we proceed to develop a suitable form of the scaling function for any two-phase material.

3.1 Scale-dependent bounds on the aggregate response

We demonstrate scale-dependent bounds of two-phase materials which are obtained by solving stochastic boundary value problems (see Figs. 3 and 4). For all volume fractions ($v_f = 0, 0.25, 0.5, 0.75, 1$), the upper and lower bounds correspond to the Voigt and Reuss estimates, respectively. Figure 3 illustrates Dirichlet and Neumann bounds on shear and bulk moduli for Ni–Cd and Sn–Ag. We observe that these bounds approach

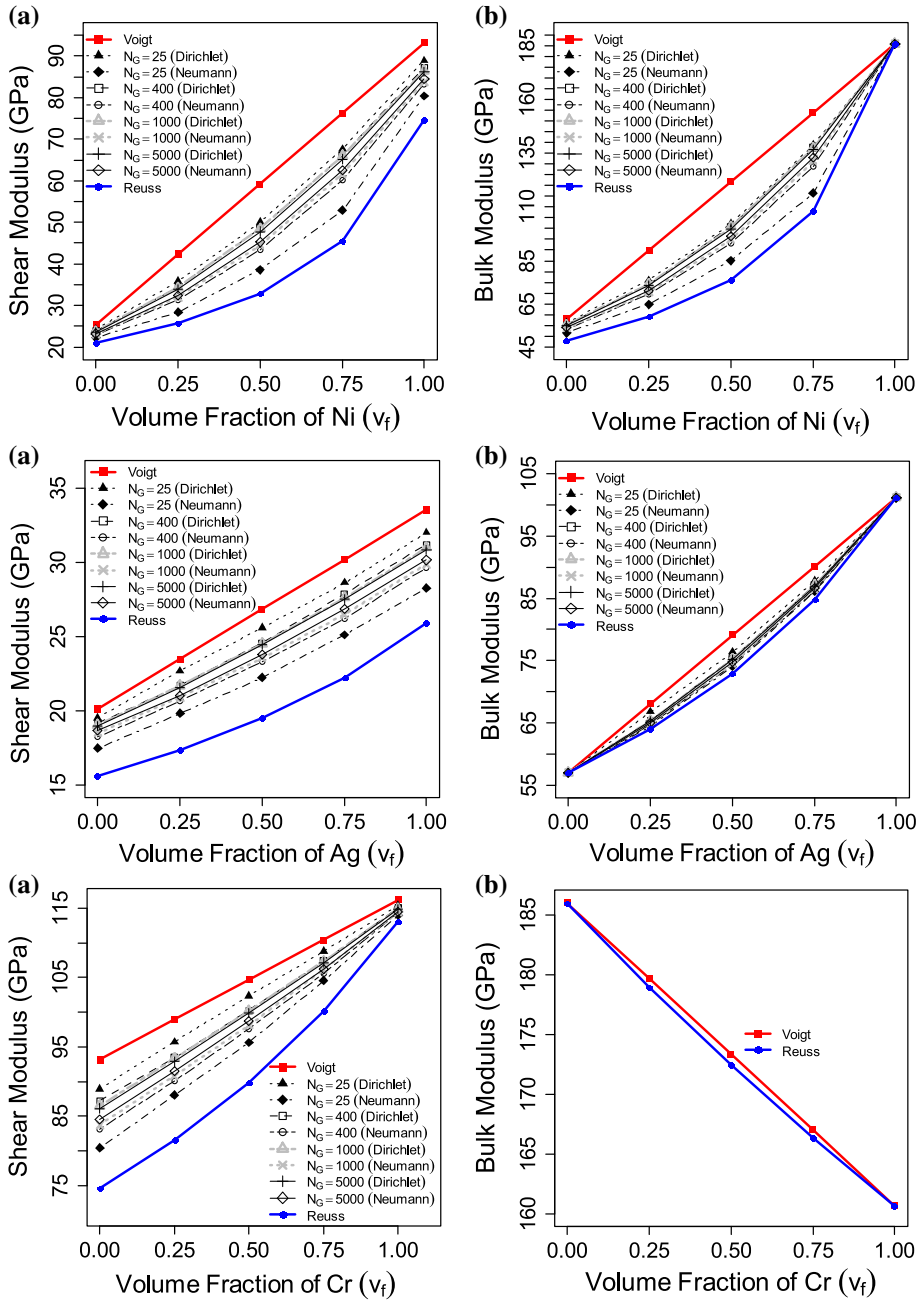

Fig. 3 Scale-dependent bounds for the Elastic Moduli of Ni–Cd (top), Sn–Ag (center) and Ni–Cr (bottom) at varying volume fractions: **a** shear modulus (GPa), **b** bulk modulus (GPa)

the effective property as the number of grains increases from 25 to 5000 at all volume fractions (see Fig. 3). Likewise, scale-dependent bounds on shear moduli of Ni–Cr (see Fig. 3) and Ni–Co (see Fig. 4) converge to the aggregate response with an increase in the number of grains. The bounds on bulk moduli for Ni–Cr are Voigt and Reuss estimates as Ni and Cr are cubic crystals (see Fig. 3). Along similar lines, upper and lower bounds on bulk moduli for Ni–Co correspond to the Voigt and Reuss averages (see Fig. 4).

Let us discuss scaling behavior of all two-phase materials (Ni–Cd, Sn–Ag, Ni–Cr, Ni–Co). Figure 5 illustrates scaling functions at various volume fractions ($v_f = 0, 0.25, 0.5, 0.75$ and 1) for these microstructures. For Ni–Cd, A_H^U is almost identical at $v_f = 0$ ($A_H^U = 1.22$) as well as $v_f = 1$ ($A_H^U = 1.25$) and therefore scaling functions are very close to each other (see Figs. 5a and e). Also, at $v_f = 0.25$ ($A_H^U = 3.77$) and

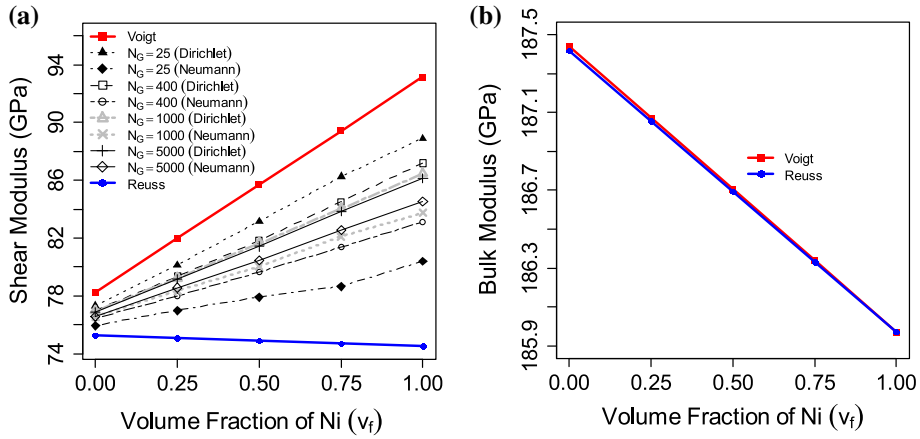

Fig. 4 Scale-dependent bounds for the Elastic Moduli of Ni–Co at varying volume fractions: **a** shear modulus (GPa), **b** bulk modulus (GPa)

$v_f = 0.75$ ($A_H^U = 3.78$), scaling functions remain the same for Ni–Cd as A_H^U is identical (see Fig. 5b and d). In addition, the scaling function for Ni–Cd at $v_f = 0.5$ can be seen in Fig. 5c. Let us now consider the scaling functions for Sn–Ag. At $v_f = 0$ ($A_H^U = 1.44$) and $v_f = 1$ ($A_H^U = 1.48$), the scaling functions are close to each other as A_H^U is similar (see Fig. 5a and e). Also, at $v_f = 0.25$ ($A_H^U = 1.84$) and $v_f = 0.75$ ($A_H^U = 1.85$), the scaling functions are the same for Sn–Ag as A_H^U is identical (see Fig. 5b and d). In addition, the scaling function for Sn–Ag at $v_f = 0.5$ can be seen in Fig. 5c. It is therefore reasonable to state that the scaling function depends only on the 'Heterogeneous Anisotropy Index' A_H^U and the mesoscale δ. By rewriting Eq. (2.20), we obtain the following:

$$f\left(C_{(1)}^{ij}, C_{(2)}^{ij}, v_f, \delta\right) \equiv f\left(A_H^U, \delta\right). \tag{3.1}$$

Along similar lines, scaling trends for Ni–Cr and Ni–Co are also identical at specific volume fractions. Figure 5b and d shows that the scaling functions are close to each other for Ni–Cr at $v_f = 0.25$ and Ni–Co at $v_f = 0.75$ as A_H^U values are 1.07 and 0.98, respectively. A similar phenomenon can be observed for Ni–Cr at $v_f = 0.5$ ($A_H^U = 0.83$) and Ni–Co at $v_f = 0.5$ ($A_H^U = 0.72$) as A_H^U values are comparable (see Fig. 5c). Likewise, the scaling functions are similar for Ni–Cr at $v_f = 0.75$ and Ni–Co at $v_f = 0.25$ as A_H^U values are 0.52 and 0.46, respectively (see Figs. 5b and d). In addition, the scaling functions for Ni–Cr and Ni–Co at $v_f = 0$ and $v_f = 1$ can be seen in Figs. 5a and e, respectively. Finally, we can also see that the scaling functions are exactly the same for Ni–Cr at $v_f = 0$ (see Fig. 5a) as well as Ni–Cd and Ni–Co at $v_f = 1$ (see Fig. 5e) as $A_H^U = 1.25$ (anisotropy of single phase Ni). In the next section, we demonstrate a specific form of the scaling function for any two-phase microstructure.

3.2 Construction of the scaling function

The functional form of the scaling function is now obtained by rewriting Eq. (2.25) as follows:

$$0 \leq \frac{1}{A_H^U} f\left(A_H^U, \delta\right) \leq 1. \tag{3.2}$$

Next, we discuss the rescaled scaling function defined in Eq. (3.2). It is important to highlight that the rescaled function is similar for all two-phase materials at various volume fractions as seen in Fig. 6. Due to the finite number of realizations used to obtain ensemble averages in this study, we observe that the curves plotted in Fig. 6 are arranged in a fusiform structure, but should converge to a single curve in the limit of an infinite set of realizations. The rescaled function, f^*, is independent of the 'Heterogeneous Anisotropy Index,' A_H^U, and is only a function of the mesoscale, δ. It is also worthwhile to mention that the existence of such an f^* is equivalent to stating that f is proportional to A_H^U. By redefining the scaling function, we obtain

$$f\left(A_H^U, \delta\right) = A_H^U f^*(\delta), \tag{3.3}$$

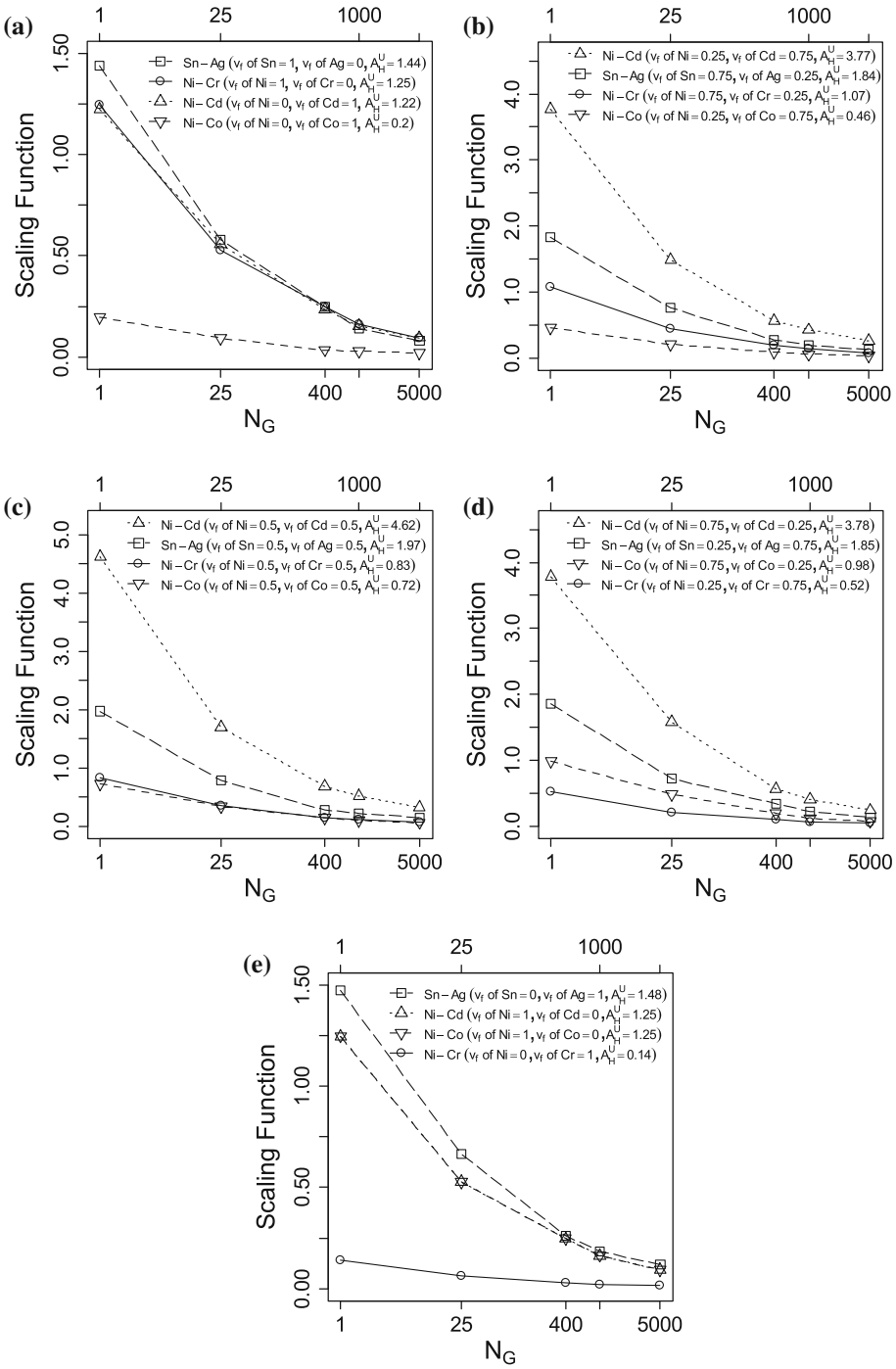

Fig. 5 Scaling Function for two-phase materials at various volume fractions **a** $v_f = 0$, **b** $v_f = 0.25$, **c** $v_f = 0.5$, **d** $v_f = 0.75$, **e** $v_f = 1$

where $f^*(\delta)$ is the material-independent rescaled function. Let us now take the average values of $f^*(\delta)$ from Fig. 6 in order to develop the effective mean rescaled function and curve fit it (see Fig. 7). It is now possible to show the following form of $f^*(\delta)$ which is based on the effective function and its fit:

$$f^*(\delta) = (\delta)^{-0.89} \tag{3.4}$$

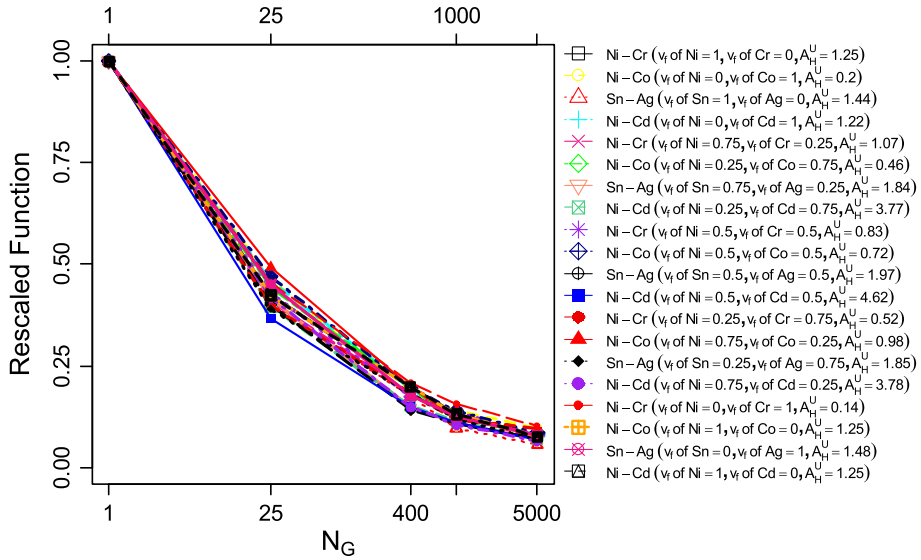

Fig. 6 Rescaled Scaling Function for two-phase materials at all volume fractions ($v_f = 0, 0.25, 0.5, 0.75, 1$)

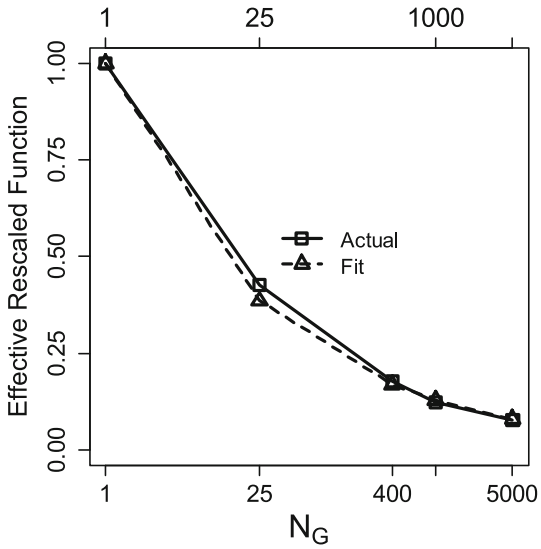

Fig. 7 Effective rescaled scaling function and fit for all two-phase materials (Ni–Cd, Sn–Ag, Ni–Cr, Ni–Co)

By using Eqs. (3.3) and (3.4), we obtain the scaling function

$$f\left(A_H^U, \delta\right) = A_H^U(\delta)^{-0.89}, \quad \delta = (N_G)^{\frac{1}{3}}. \tag{3.5}$$

At this stage, we reconstruct the scaling function using Eq. (3.5) for all two-phase polycrystals (Ni–Cd, Sn–Ag, Ni–Cr, Ni–Co) at different volume fractions ($v_f = 0, 0.25, 0.5, 0.75, 1$) as shown in Fig. 8. It is evident from this plot that this formulation captures the scaling function accurately for all two-phase materials at several volume fractions.

4 Material scaling diagram

The power-law form of the scaling function given in Eq. (3.5) is employed in order to construct contours in (A_H^U, N_G) space as shown in Fig. 9. It is clear that the curves shift toward higher grain sizes as scaling function decreases (from $f = 0.23$ to $f = 0.01$) and vice versa. We have also seen that the scaling function is zero

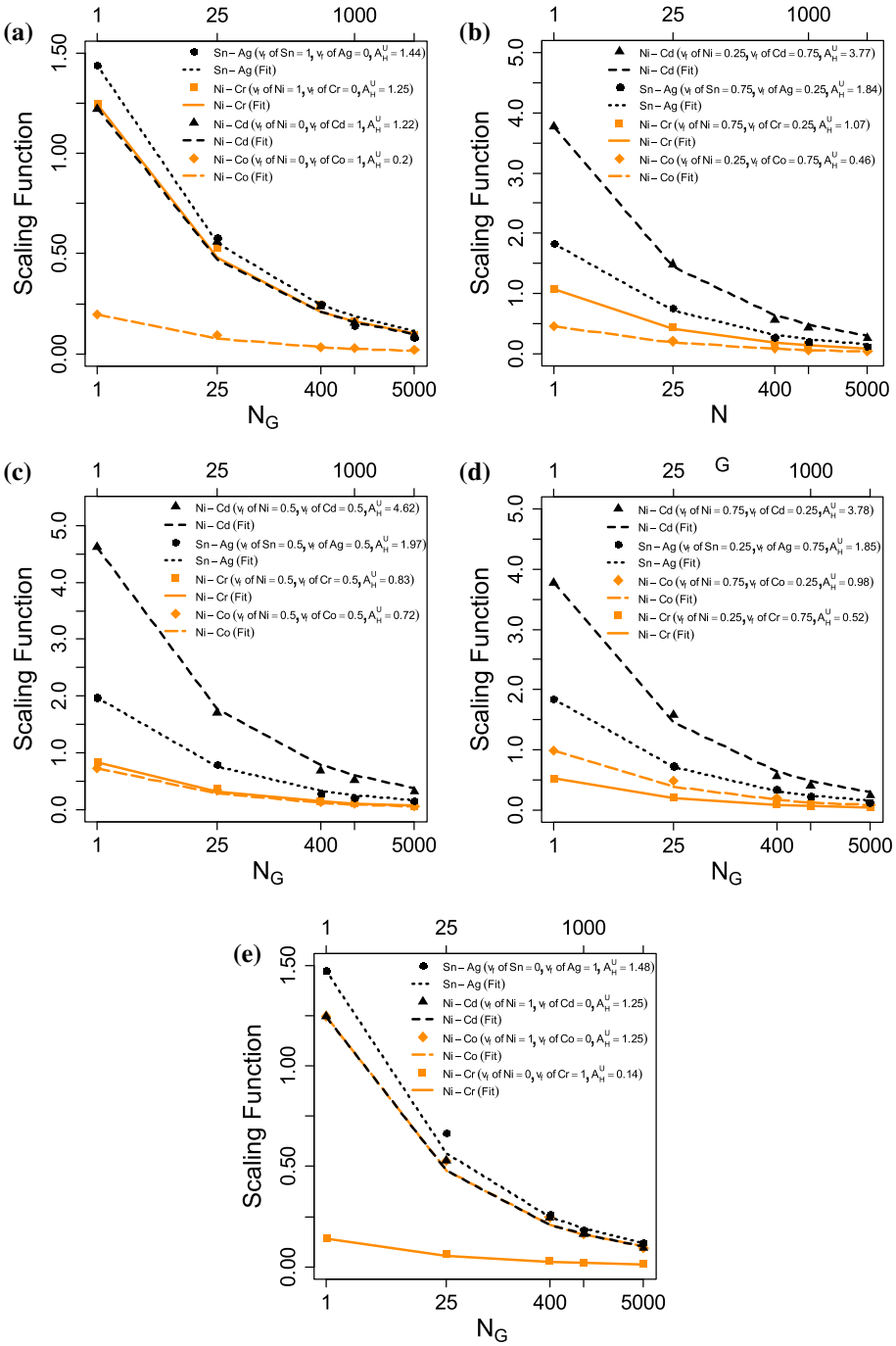

Fig. 8 Scaling function and fit for two-phase materials at various volume fractions **a** $v_f = 0$, **b** $v_f = 0.25$, **c** $v_f = 0.5$, **d** $v_f = 0.75$, **e** $v_f = 1$

at infinite grain sizes. One can now select a specific value of scaling function in order to determine the grain sizes required for homogenization. We illustrate this concept by choosing a finite value of scaling function ($f = 0.2$) and develop Fig. 10 for several two-phase materials (Ni–Cd, Sn–Ag, Ni–Cr, Ni–Co) at various volume fractions ($vf = 0, 0.25, 0.5, 0.75, 1$). We observe that for a highly anisotropic two-phase material (Ni–Cd with an $A_H^U = 4.62$), homogeneity can be achieved at $N_G = 39835$ ($\delta \cong 35$). Similarly, for Sn–Ag at a $v_f = 0.5$ and $A_H^U = 1.97$, aggregate response can be determined at $N_G = 2255$ ($\delta \cong 14$). Finally, for a two-phase polycrystal with low anisotropy (Ni–Cr with an $A_H^U = 0.14$), the number of grains required for homogenization is $N_G = 1$ ($\delta = 1$).

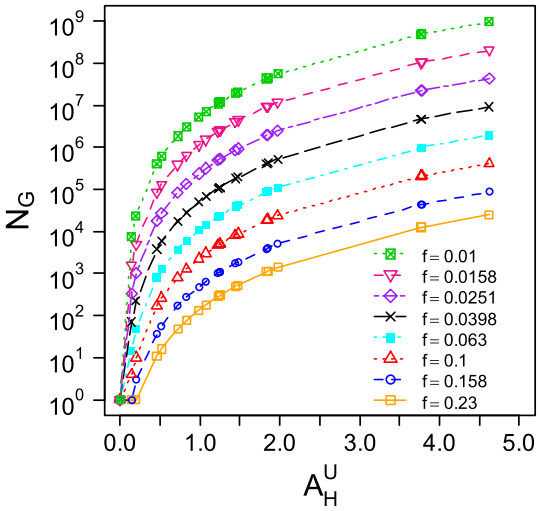

Fig. 9 Contours of the scaling function for $0.01 \leq f \leq 0.23$

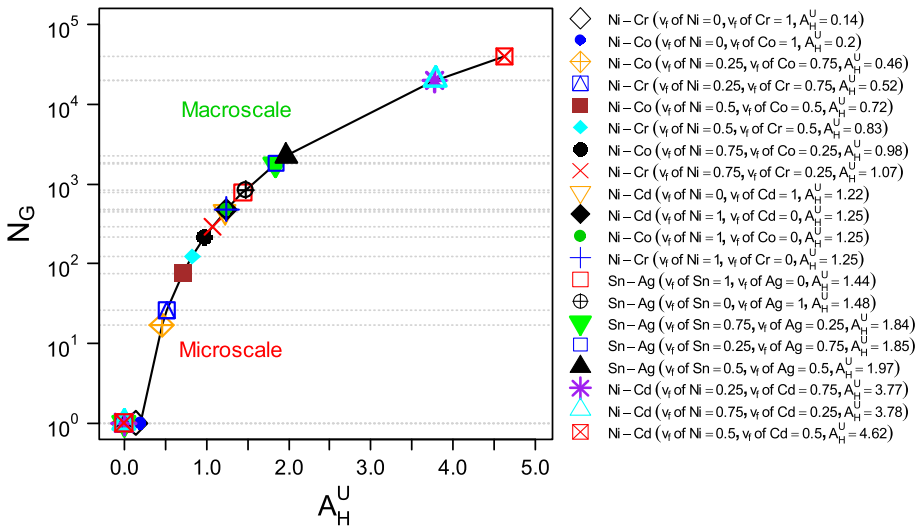

Fig. 10 Material scaling diagram at $f = 0.2$

5 Conclusion

In conclusion, we have illustrated the procedure to obtain scale-dependent bounds on the elastic response of two-phase random polycrystals by solving Dirichlet and Neumann type boundary value problems (9250) which are consistent with the Hill–Mandel homogenization condition. It was also shown that a variety of two-phase materials (Ni–Cd, Sn–Ag, Ni–Cr, Ni–Co) at different volume fractions ($v_f = 0$, 0.25, 0.5, 0.75, 1) can be studied together in terms of the elastic scaling function. This form of the scaling function consists of the 'Heterogeneous Anisotropy Index (A_H^U)' and the number of grains in a microstructure. Some of the properties of the scaling function were demonstrated as follows: (i) the scaling function is zero when the grain sizes are infinite; (ii) the scaling function remains the same when it is multiplied by a real number, α; (iii) the scaling function behaves as the Universal Anisotropy Index when the volume fractions are 0 and 1. We also developed a material scaling diagram for any two-phase material which can be used for estimating the grain size required for homogenization. In this study, we have analyzed only two of the three boundary conditions that emerge on account of the Hill–Mandel condition. One can also consider the elastic response of two-phase materials subjected to the mixed-orthogonal boundary condition. Finally, to the best of our knowledge, this is the first attempt for analyzing the scaling behavior of two-phase random polycrystals.

References

1. Ranganathan, S.I., Ostoja-Starzewski, M.: Universal elastic anisotropy index. Phys. Rev. Lett. **101**(5), 055504 (2008)
2. Ostoja-Starzewski, M., Kale, S., Karimi, P., Malyarenko, A., Raghavan, B., Ranganathan, S.I., Zhang, J.: Chapter two-scaling to RVE in random media. Adv. Appl. Mech. **49**, 111–211 (2016)
3. Ostoja-Starzewski, M., Ranganathan, S.I.: Scaling and homogenization in spatially random composites. Mathematical Methods and Models in Composites, pp. 61–101. Imperial College Press, London (2013)
4. Zhang, J., Chen, Z., Dong, C.: Simulating intergranular stress corrosion cracking in AZ31 using three-dimensional cohesive elements for grain structure. J. Mater. Eng. Perform. **24**(12), 4908–4918 (2015)
5. Murshed, M.R., Ranganathan, S.I., Abed, F.H.: Design maps for fracture resistant functionally graded materials. Eur. J. Mech. A. Solids **58**, 31–41 (2016)
6. Oezelt, H., Kovacs, A., Wohlhüter, P., Kirk, E., Nissen, D., Matthes, P., Heyderman, L.J., Albrecht, M., Schrefl, T.: Micromagnetic simulation of exchange coupled ferri-/ferromagnetic composite in bit patterned media. J. Appl. Phys. **117**(17), 28–33 (2015)
7. Toifl, M., Meisels, R., Hartlieb, P., Kuchar, F., Antretter, T.: 3D numerical study on microwave induced stresses in inhomogeneous hard rocks. Miner. Eng. **90**, 29–42 (2016)
8. Sledzinska, M., Graczykowski, B., Placidi, M., Reig, D .S., Sachat, A El, Reparaz, J., Alzina, F., Mortazavi, B., Quey, R., Colombo, L., et al.: Thermal conductivity of MoS_2 polycrystalline nanomembranes. 2D Materials **3**(3), 035016 (2016)
9. Ardeljan, M., Beyerlein, I.J., Knezevic, M.: A dislocation density based crystal plasticity finite element model: application to a two-phase polycrystalline HCP/BCC composites. J. Mech. Phys. Solids **66**, 16–31 (2014)
10. Hashin, Z., Shtrikman, S.: A variational approach to the theory of the elastic behaviour of multiphase materials. J. Mech. Phys. Solids **11**(2), 127–140 (1963)
11. Walpole, L.: On the overall elastic moduli of composite materials. J. Mech. Phys. Solids **17**(4), 235–251 (1969)
12. Watt, J.P., Davies, G.F., O'Connell, R.J.: The elastic properties of composite materials. Rev. Geophys. **14**(4), 541–563 (1976)
13. Mori, T., Tanaka, K.: Average stress in matrix and average elastic energy of materials with misfitting inclusions. Acta Metall. **21**(5), 571–574 (1973)
14. Benveniste, Y.: A new approach to the application of Mori–Tanaka's theory in composite materials. Mech. Mater. **6**(2), 147–157 (1987)
15. Weng, G.: The theoretical connection between Mori–Tanaka's theory and the Hashin–Shtrikman–Walpole bounds. Int. J. Eng. Sci. **28**(11), 1111–1120 (1990)
16. Ni, Y., Chiang, M.Y.: Prediction of elastic properties of heterogeneous materials with complex microstructures. J. Mech. Phys. Solids **55**(3), 517–532 (2007)
17. Eshelby, J.D.: The determination of the elastic field of an ellipsoidal inclusion, and related problems. In: Proceedings of the Royal Society of London A: Mathematical, Physical and Engineering Sciences, vol. 241, pp. 376–396. The Royal Society (1957)
18. Hill, R.: Elastic properties of reinforced solids: some theoretical principles. J. Mech. Phys. Solids **11**(5), 357–372 (1963)
19. Mandel, J.: Contribution théorique à l'étude de l'écrouissage et des lois de l'écoulement plastique. In: Applied Mechanics, pp. 502–509. Springer (1966)
20. Ranganathan, S.I., Ostoja-Starzewski, M.: Scaling function, anisotropy and the size of RVE in elastic random polycrystals. J. Mech. Phys. Solids **56**(9), 2773–2791 (2008)
21. Ranganathan, S.I., Ostoja-Starzewski, M.: Towards scaling laws in random polycrystals. Int. J. Eng. Sci. **47**(11), 1322–1330 (2009)
22. Murshed, M.R., Ranganathan, S.I.: Hill–Mandel condition and bounds on lower symmetry elastic crystals. Mech. Res. Commun. **81**, 7–10 (2017)
23. Dalaq, A.S., Ranganathan, S.I.: Invariants of mesoscale thermal conductivity and resistivity tensors in random checkerboards. Eng. Comput. **32**(6), 1601–1618 (2015)
24. Kale, S., Saharan, A., Koric, S., Ostoja-Starzewski, M.: Scaling and bounds in thermal conductivity of planar Gaussian correlated microstructures. J. Appl. Phys. **117**(10), 104301 (2015)
25. Ostoja-Starzewski, M., Schulte, J.: Bounding of effective thermal conductivities of multiscale materials by essential and natural boundary conditions. Phys. Rev. B **54**(1), 278 (1996)
26. Du, X., Ostoja-Starzewski, M.: On the scaling from statistical to representative volume element in thermoelasticity of random materials. Netw. Heterog. Media **1**(2), 259 (2006)
27. Khisaeva, Z., Ostoja-Starzewski, M.: Mesoscale bounds in finite elasticity and thermoelasticity of random composites. In: Proceedings of the Royal Society of London A: Mathematical, Physical and Engineering Sciences, vol. 462, pp. 1167–1180. The Royal Society (2006)
28. Ostoja-Starzewski, M.: Material spatial randomness: from statistical to representative volume element. Probab. Eng. Mech. **21**(2), 112–132 (2006)
29. Ostoja-Starzewski, M., Du, X., Khisaeva, Z., Li, W.: Comparisons of the size of the representative volume element in elastic, plastic, thermoelastic, and permeable random microstructures. Int. J. Multiscale Comput. Eng. **5**(2), 73–82 (2007)
30. Du, X., Ostoja-Starzewski, M.: On the size of representative volume element for darcy law in random media. In: Proceedings of the Royal Society of London A: Mathematical, Physical and Engineering Sciences, vol. 462, pp. 2949–2963. The Royal Society (2006)
31. Ostoja-Starzewski, M.: Microstructural Randomness and Scaling in Mechanics of Materials. CRC Press, Boca Raton (2007)
32. Ranganathan, S.I., Ostoja-Starzewski, M.: Scale-dependent homogenization of inelastic random polycrystals. J. Appl. Mech. **75**(5), 051008 (2008)
33. Ostoja-Starzewski, M.: Scale effects in plasticity of random media: status and challenges. Int. J. Plast **21**(6), 1119–1160 (2005)
34. Kanit, T., Forest, S., Galliet, I., Mounoury, V., Jeulin, D.: Determination of the size of the representative volume element for random composites: statistical and numerical approach. Int. J. Solids Struct. **40**(13), 3647–3679 (2003)

35. Voigt, W.: Lehrbuch der Kristallphysik (mit Ausschluss der Kristalloptik). Teubner, Leipzig (1928)
36. Reuss, A.: Berechnung der fließgrenze von mischkristallen auf grund der plastizitätsbedingung für einkristalle. ZAMM J. Appl. Math. Mech./Z. Angew. Math. Mech. **9**(1), 49–58 (1929)
37. Kanit, T., N'Guyen, F., Forest, S., Jeulin, D., Reed, M., Singleton, S.: Apparent and effective physical properties of heterogeneous materials: representativity of samples of two materials from food industry. Comput. Methods Appl. Mech. Eng. **195**(33), 3960–3982 (2006)
38. Murshed, M.R., Ranganathan, S.I.: Scaling laws in elastic polycrystals with individual grains belonging to any crystal class. Acta Mech. **228**(4), 1525–1539 (2017)
39. Ranganathan, S.I., Ostoja-Starzewski, M.: Mesoscale conductivity and scaling function in aggregates of cubic, trigonal, hexagonal, and tetragonal crystals. Phys. Rev. B **77**(21), 214308 (2008)
40. Raghavan, B.V., Ranganathan, S.I.: Bounds and scaling laws at finite scales in planar elasticity. Acta Mech. **225**(11), 3007–3022 (2014)
41. Dalaq, A.S., Ranganathan, S.I., Ostoja-Starzewski, M.: Scaling function in conductivity of planar random checkerboards. Comput. Mater. Sci. **79**, 252–261 (2013)
42. Raghavan, B.V., Ranganathan, S.I., Ostoja-Starzewski, M.: Electrical properties of random checkerboards at finite scales. AIP Adv. **5**(1), 017131 (2015)
43. Zhang, J., Ostoja-Starzewski, M.: Frequency-dependent scaling from mesoscale to macroscale in viscoelastic random composites, In: Proceedings of the Royal Society of London A: Mathematical, Physical and Engineering Sciences, vol. 472. The Royal Society (2016)
44. Norian, K.: Equivalent circuit components of nickel–cadmium battery at different states of charge. J. Power Sources **196**(11), 5205–5208 (2011)
45. Wang, Y., Lu, K.H., Gupta, V., Stiborek, L., Shirley, D., Chae, S.-H., Im, J., Ho, P.S.: Effects of Sn grain structure on the electromigration of Sn–Ag solder joints. J. Mater. Res. **27**(08), 1131–1141 (2012)
46. Kazi, I.H., Wild, P., Moore, T., Sayer, M.: Characterization of sputtered nichrome (Ni–Cr 80/20 wt%) films for strain gauge applications. Thin Solid Films **515**(4), 2602–2606 (2006)
47. Srivastava, M., Selvi, V.E., Grips, V.W., Rajam, K.: Corrosion resistance and microstructure of electrodeposited nickel–cobalt alloy coatings. Surf. Coat. Technol. **201**(6), 3051–3060 (2006)
48. Hill, R.: The Mathematical Theory of Plasticity. Oxford University Press, Oxford (1950)
49. Quey, R., Dawson, P., Barbe, F.: Large-scale 3D random polycrystals for the finite element method: generation, meshing and remeshing. Comput. Methods Appl. Mech. Eng. **200**(17), 1729–1745 (2011)
50. El Houdaigui, F., Forest, S., Gourgues, A.-F., Jeulin, D.: On the size of the representative volume element for isotropic elastic polycrystalline copper. In: IUTAM Symposium on Mechanical Behavior and Micro-Mechanics of Nanostructured Materials, pp. 171–180. Springer (2007)
51. Walpole, L.: Elastic behavior of composite materials: theoretical foundations. Adv. Appl. Mech. **21**, 169–242 (1981)
52. Walpole, L.: Fourth-rank tensors of the thirty-two crystal classes: multiplication tables. In: Proceedings of the Royal Society of London A: Mathematical, Physical and Engineering Sciences, vol. 391, pp. 149–179. The Royal Society (1984)
53. Hill, R.: Continuum micro-mechanics of elastoplastic polycrystals. J. Mech. Phys. Solids **13**(2), 89–101 (1965)
54. Ranganathan, S.I., Ostoja-Starzewski, M., Ferrari, M.: Quantifying the anisotropy in biological materials. J. Appl. Mech. **78**(6), 064501 (2011)
55. Itskov, M.: On the theory of fourth-order tensors and their applications in computational mechanics. Comput. Methods Appl. Mech. Eng. **189**(2), 419–438 (2000)
56. Sab, K.: On the homogenization and the simulation of random materials. Eur. J. Mech. A/Solids **11**(5), 585–607 (1992)
57. Huet, C.: Application of variational concepts to size effects in elastic heterogeneous bodies. J. Mech. Phys. Solids **38**(6), 813–841 (1990)
58. Hill, R.: The elastic behaviour of a crystalline aggregate. Proc. Phys. Soc. Lond Sect A **65**(5), 349–354 (1952)